Supporting Information

Multiligand Coordination Self-assembly Bimetallic Complex Derived FeC_x Decorate Fe and N Co-doped Carbon Nanotube for Highly Efficient Oxygen Reduction Reaction

Qiulin Li,[a,c] Zhiqin Deng,[b] Yan-Dong Ma,[a,c] Yangyang Tan,[a,c] Ruilin He,[a,c] Qianwen Chen,[a,c] Shu-Juan Bao,[a,c] * and Heng Liu[b]*

[a]Institute for Clean Energy and Advanced Materials, School of Materials and Energy, Southwest University, Chongqing 400715, China

[b]School of Chemistry and Chemical Engineering, University of South China, Hengyang 421001, Hunan, China

[c]Chongqing Key Lab for Battery Materials and Technologies, Southwest University, Chongqing 400715, P. R. China

*Corresponding author.

E-mail: liuheng419@usc.edu.cn, baoshj@swu.edu.cn

Experimental section

Chemicals

Anhydrous Zinc Chloride ($ZnCl_2$), Ferric Chloride ($FeCl_3$), 2-Methylimidazole (MeIM), Potassium ferricyanide ($K_3[Fe(CN)_6]$), and 2-isopropanol were purchased from Aladdin Industrial Co., methanol was purchased from Sinopharm Chemical Reagent Co., Nafion solution (5 wt%) was purchased from Sigma-Aldrich. All chemicals were analytical grade and used as received without further purification.

Catalyst synthesis

Synthesis of FeZn-PBMI，FeZn-PBAs and ZIF-8:

In details, 3 g of 2-methylimidazole and 1.97 g of $K_3[Fe(CN)_6]$ were dissolved in 500 mL of ultrapure water with continuous stirring referred to as solution A, and then 1.632 g of anhydrous $ZnCl_2$ was dissolved in 100 mL of methanol was drop by drop added into solution A and constant stirring for 12 hours. Further, the resulting mixture was centrifuged and washed four times using a 5:1 (v/v) mixture of ultrapure water and methanol. The final product was dried overnight in a vacuum oven at 60 °C and named as FeZn-PBMI. As comparison, the synthesis procedure for ZIF-8 and FeZn-PBAs followed the same protocol as for FeZn-PBMI, except without the addition of $K_3[Fe(CN)_6]$ or 2-methylimidazole.

Synthesis of Fe_xC@FeNCNTs, Fe_xC@FeNC and NPC:

the FeZn-PBMI, FeZn-PBAs and ZIF-8 were subjected to annealing in a tube furnace under an Ar atmosphere and firstly carbonized at 400 °C for 1 h, and then continued to be carbonized at 800 °C for 2 h, the heating rates were controlled at 5 °C min^{-1} for the first stage and 2 °C min^{-1} for the second stage, the obtained product has not been subjected to acid corrosion and secondary carbonization treatment.

Structural and composition characterization

The morphological structures of the resulting catalysts were investigated by field-emission scanning electron microscopy (FESEM, JEOL-7800F) and transmission electron microscope (TEM, JEM-2100F). X-ray diffraction (XRD) patterns were obtained with XRD-7000 (XRD, Shimadzu XRD-7000) with Cu K_α source radiation at

a scanning rate of 5° min^{-1} from 5 to 90°. The surface compositions of the resultant catalysts were studied by X-ray photoelectron spectroscopy (XPS, Escalab 250xi, Thermo Scientific). N_2 sorption was carried out with ASAP 2020 to measure Brunauer-Emmett-Teller (BET) surface area and pore size distribution.

Electrochemical measurements

5 mg of catalysts powder was ultrasonically dispersed in a mixture of 2-isopropanol-H_2O (1 mL, v/v=1:1) containing 50 μL of 5 wt% Nafion solution. Then, 10 μL of the catalyst ink was loaded onto a glassy carbon electrode (D = 5.0 mm) of a rotation ring-disk electrode (RRDE) with a catalyst loading of 0.2 mg cm^{-2} as working electrode. For comparison, commercial 20 wt% Pt/C ink was prepared by the same method. All electrochemical measurements were carried on Autolab bi-potential electrochemical workstation (Metrohm). Graphite rod and Ag/AgCl were used as counter electrode and reference electrode, respectively. The number of electron transferred (n) and kinetic current density (J_k) were calculated from the Koutecky-Levich equation:

$$\frac{1}{J}=\frac{1}{J_L}+\frac{1}{J_K}=\frac{1}{B\omega^{1/2}}+\frac{1}{J_K} \quad (1)$$

$$B = 0.2nFC_0D^{2/3}\upsilon^{-1/6} \quad (2)$$

where J is the measured current density, J_L is the diffusion limiting current density, ω is the angular velocity of the disk, F is the Faraday constant (96485 C mol^{-1}), C_0 is the bulk concentration of oxygen (1.2×10^{-6} mol cm^{-1}), D is the diffusion coefficient of oxygen (1.9×10^{-5} cm^2 s^{-1}), υ is the he kinetic viscosity (0.01 cm^2 s^{-1}), and n is the number of electron transferred during the ORR process. The number of electron transferred can also be calculated from the RRDE measurement according to the following equation:

$$n = 4 \times \frac{I_{disk}}{I_{disk} + I_{ring}/N} \quad (3)$$

where I_{disk} is the measured current of disk electrode, I_{ring} is the measured current of Pt ring electrode, and N is the current collection efficiency of Pt ring.

Cyclic voltammetry (CV) tests were conducted on various electrodes in a solution

containing 0.2 M $[Fe(CN)_6]^{3-/4-}$ as a redox probe and 0.1 M KCl as a electrolyte, at a scan rate of 20 mV s^{-1}. Typically, the CV peak area is directly proportional to the redox reaction of $[Fe(CN)_6]^{3-/4-}$ occurring on the electrode, where a larger peak area suggests a greater available surface area for the redox reaction, allowing for qualitative assessment of the catalyst specific surface area. A smaller ΔE_p (the potential difference between the anodic and cathodic peaks) indicates rapid electron transfer kinetics at the electrode, which can be used to qualitatively analyze the kinetics of reactions occurring on the electrode. Furthermore, the specific capacitance of the material can be evaluated using the following equation.

$$C = \frac{1}{m\upsilon\,(V_c - V_{a)}} \int_{V_a}^{V_c} IdV \qquad (4)$$

C (F g^{-1}) represents the specific capacitance, m (g) denotes the mass of the electroactive material, and υ (mV s^{-1}) refers to the scan rate. V_c and V_a correspond to the upper and lower potential limits of the CV test, respectively. I (A) indicates the instantaneous current along the CV curve.

Zn−air battery test

The Zn-air battery was evaluated using an electrolyte mixture of 6.0 M KOH and 0.2 M $Zn(CH_3COO)_2$. The 0.2 mm thick Zn sheet served as negative electrode, and the surface oxide layer was removed by sandpaper before use. The air side electrode base material was prepared by rolling the hydrophobic carbon paper, waterproof and breathable membrane (purchased from Changsha spring Co.) and foam nickel catalyst together. After coating the catalyst on the carbon paper, the composite electrode material was obtained as the air cathode, wherein the load of Fe_xC@FeNCNTs was 2.0 mg cm^{-2}. All Zn–air batteries were evaluated under ambient conditions. The polarization curves were recorded by linear sweep voltammetry (5 mV s^{-1}, at room temperature) on a CHI 760E workstation (CH Instrument Co.), charge/discharge cycling curves were recorded by a LAND CT2001 battery test system (Wuhan Kingnuo Electronic Co.).

The calculation formula for power density is:

$$Power\ density = Current\ density \times Voltage \quad (5)$$

The round-trip efficiency is calculated by the following formula:

$$Round - trip\ efficiency = \frac{Discharge\ platform\ voltage}{Charge\ platform\ voltage} \times \quad (6)$$

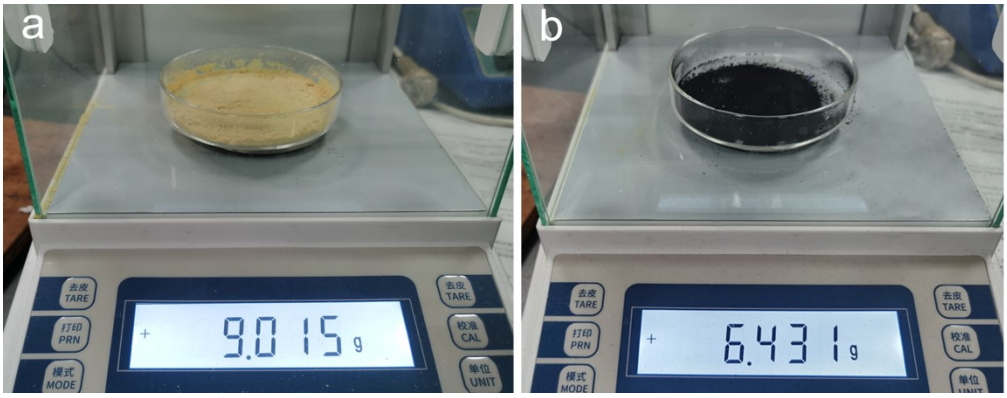

Figure S1. Photograph of the precursor (a) FeZn-PBMI and (b) Fe_xC@FeNCNTs.

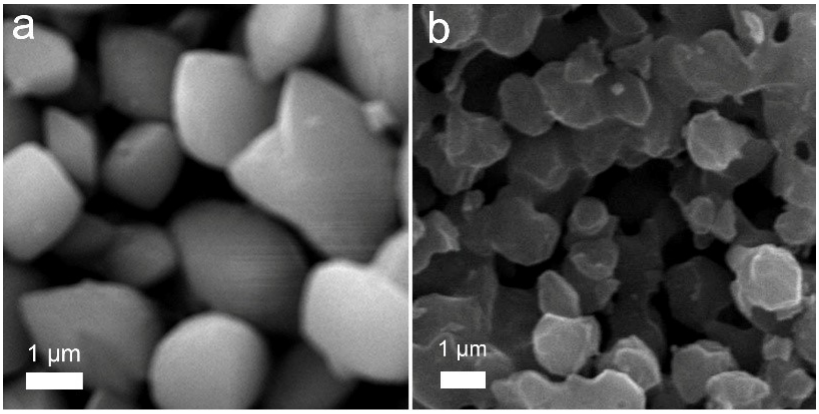

Figure S2. SEM images of (a) ZIF-8 and (b) NPC.

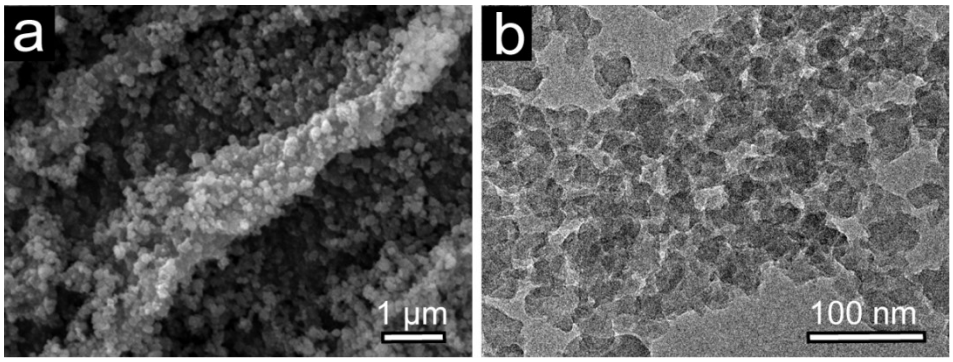

Figure S3. (a) SEM and (b) TEM images of the FeZn-PBMI.

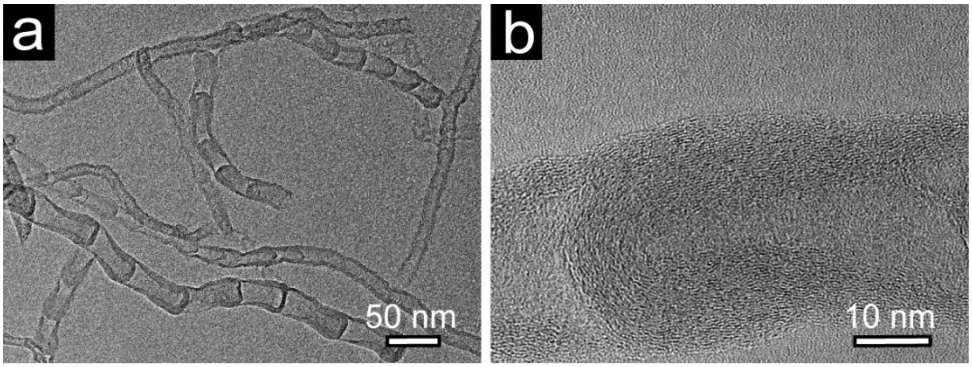

Figure S4. (a) TEM and (b) HRTEM images of the resultant Fe_xC@FeNCNTs.

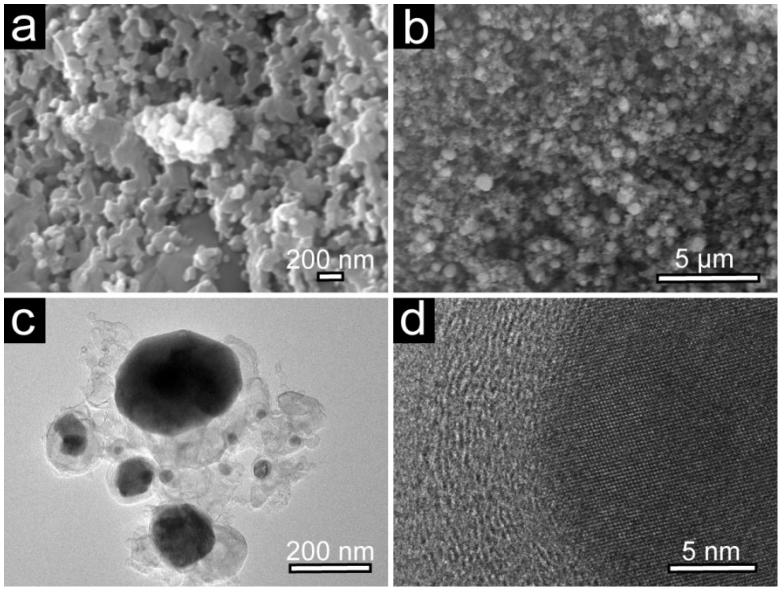

Figure S5. SEM images of (a) FeZn-PBAs and (b-d) Fe_xC@FeNC.

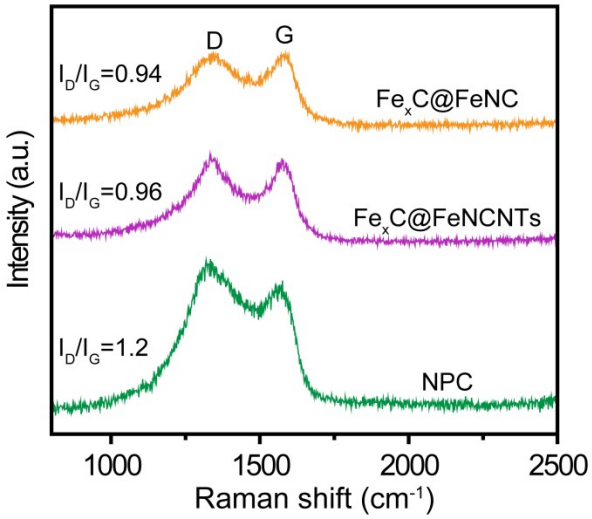

Figure S6 Raman spectrum of NPC, Fe_xC@FeNC and Fe_xC@FeNCNTs.

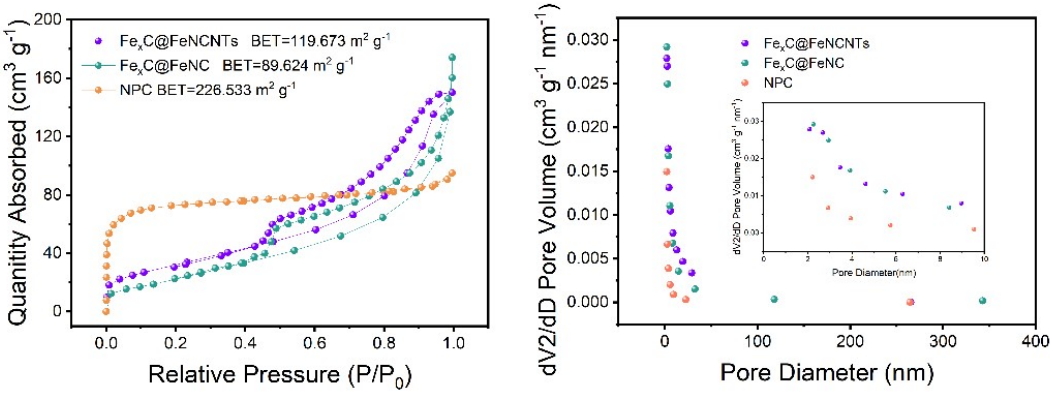

Figure S7. (a) N_2 sorption isotherms and (b) pore size distributions of NPC, Fe_xC@FeNC and Fe_xC@FeNCNTs.

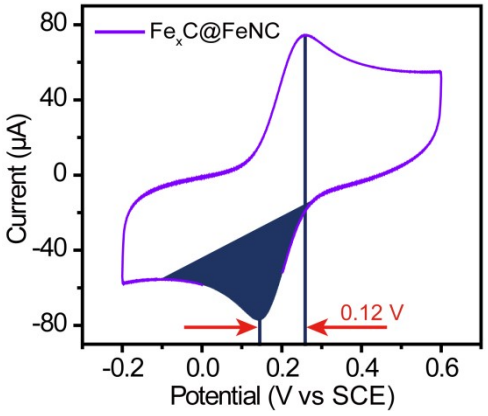

Figure S8 CV curves of Fe_xC@FeNC in a solution containing 0.2 M $[Fe(CN)_6]^{3-/4-}$ as the redox probe and 0.1 M KCl as the supporting electrolyte.

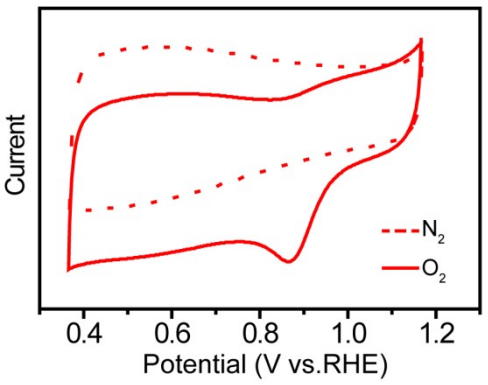

Figure S9. CV curves of the resultant Fe_xC@FeNCNTs in N_2 and O_2-saturated 0.1 M KOH.

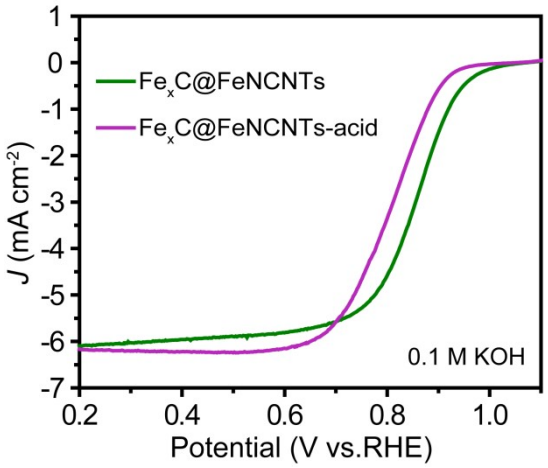

Figure S10. LSV curves of Fe_xC@FeNCNTs and leached by 0.5 M H_2SO_4 for 12 h and the resulting material is denoted as Fe_xC@FeNCNTs-acid at an RDE rotation speed of 1600 rpm with a scan rate of 5 mV s^{-1} in O_2 saturated 0.1 M KOH.

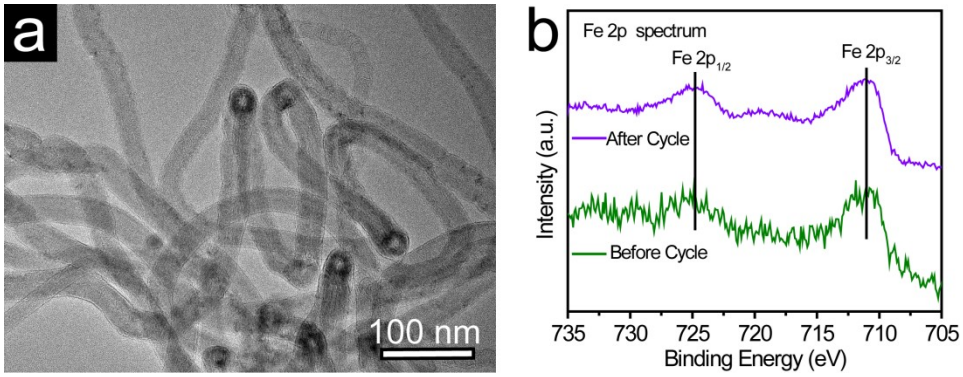

Figure S11. (a) TEM image of after stability tested Fe_xC@FeNCNTs, and (b) High-resolution Fe 2p XPS spectra of intial and after stability tested Fe_xC@FeNCNTs.

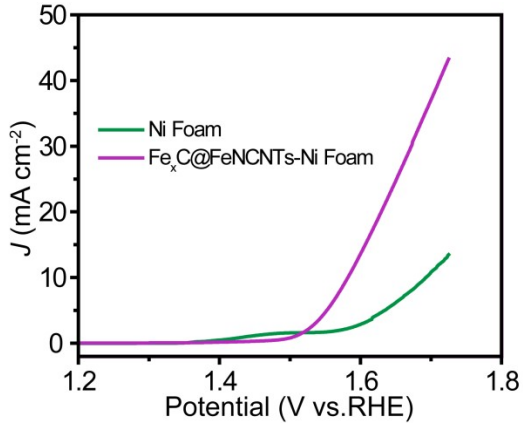

Figure S12 Polarization curves of Fe_xC@FeNCNTs with a scan rate of 10 mV s^{-1} in 1 M KOH solution.

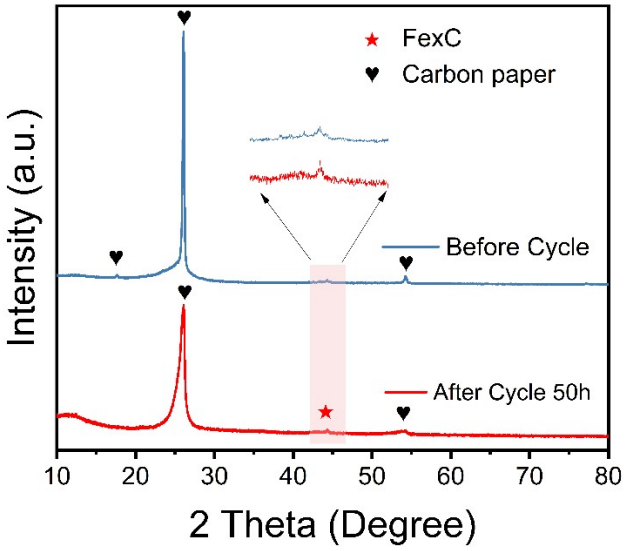

Figure S13. XRD patterns of Fe_xC@FeNCNTs before and after 50 h cycles test.

Table S1 Comparison of ORR catalytic performances between Fe_xC@FeNCNTs and the catalysts in the literature (0.1 M KOH, 1600 rpm).

catalysts	Loading [mg/cm^2]	E_{onset} [V vs. RHE]	$E_{1/2}$ [V vs. RHE]	Reference
Fe_xC@FeNCNTs	0.20	1.03	0.87	This work
CoSA@NPC	0.40	0.99	0.878	[1]
Fe-AC-2	0.20	1.00	0.87	[2]
FeN_5-C/G	0.255	0.96	0.84	[3]
Sb_1/NG(O)	0.255	1.03	0.86	[4]
Fe-NiNC-50	0.25	1.0	0.85	[5]
Fe-N-C/FeN	1.00	0.96	0.81	[6]
FeCo-NSC	0.40	~0.98	0.86	[7]
FeSA/HNPC	0.20	0.92	0.83	[8]
Mn-SA@CNSs	0.255	0.96	0.88	[9]
Fe_3C/NG-800	0.40	~0.96	0.86	[10]
Co/CoFe@NC	0.25	0.97	0.84	[11]
Fe@N-CNT/NS	0.20	1.0	0.82	[12]
Fe-SAs@NCTCs	0.255	0.90	0.80	[13]
Co@NSC-acid	0.20	0.92	0.82	[14]
Co-Cat-T550	0.45	0.96	0.86	[15]
Co-NCS-2	0.20	0.96	0.90	[16]
Mn Sas-N_4	0.15	~1.00	0.90	[17]
Fe/NC-3	0.30	0.97	0.90	[18]
Fe-SAs@NCTCs	0.255	1.02	0.91	[19]
Se@NC-1000	0.50	0.95	0.85	[20]

References

[1] L. Li, X. Liu, J. Wang, R. Liu, Y. Liu, C. Wang, W. Yang, X. Feng, B. Wang, *J. Mater. Chem. A* **2022**, *10*, 18723-18729.

[2] Y. Wang, Q. Li, L.-c. Zhang, Y. Wu, H. Chen, T. Li, M. Xu, S.-J. Bao, *J. Mater. Chem. A* **2021**, *9*, 7137-7142.

[3] H. Zhang, S. Jia, X. Shi, Z. Li, B. Liu, N. Li, Y. Li, S. Hu, H. Wang, *Mater. Chem. Front.* **2021**, *5*, 8127-8137.

[4] Y. Gu, B.J. Xi, H. Zhang, Y.C. Ma, S.L. Xiong, *Angew. Chem. Int. Ed.* **2022**, 134, e202202200.

[5] X. Zhu, D. Zhang, C.-J. Chen, Q. Zhang, R.-S. Liu, Z. Xia, L. Dai, R. Amal, X. Lu, *Nano Energy* **2020**, 71, 104597.

[6] X. Luo, X. Wei, H. Wang, W. Gu, T. Kaneko, Y. Yoshida, X. Zhao, C. Zhu, *Nano-Micro Lett.* **2020**, *12*, 163.

[7] Y. Wu, C. Ye, L. Yu, Y. Liu, J. Huang, J. Bi, L. Xue, J. Sun, J. Yang, W. Zhang, X. Wang, P. Xiong, J. Zhu, *Energy Storage Mater.* **2022**, 45, 805-813.

[8] X. Jin, Y. Xie, J. Fu, C. Zhao, Y. Xu, Y. Lv, B. Zhang, K. Sun, R. Si, J. Huang, *ChemCatChem* 2021, 13, 2683-2690.

[9] L. Zong, F. Lu, W. Zhang, K. Fan, X. Chen, B. Johannessen, D. Qi, N.M. Bedford, M. Warren, C.U. Segre, P. Liu, L. Wang, H. Zhao, *Energy Storage Mater.* **2023**, 49, 209-218.

[10] M. Xiao, J. Zhu, L. Feng, C. Liu, W. Xing, Adv. Mater. 2015, 27, 2521-2527.

[11] Y. Niu, X. Teng, S. Gong, M. Xu, S. G. Sun, Z. Chen, *Nano-Micro Lett.* **2021**, *13*, 126.

[12] X. Li, L. Ni, J. Zhou, L. Xu, C. Lu, G. Yang, W. Ding, W. Hou, *Nanoscale* **2020**, 12, 13987-13995.

[13] F. Lu, K. Fan, L. Cui, B. Li, Y. Yang, L. Zong, L. Wang, *Appl. Catal. B-Environ.* **2022**, 313, 121464.

[14] Z.-y. Chen, H. Liu, L.-c. Zhang, Q.-l. Li, M.-w. Xu, S.-J. Bao, *ACS Sustain. Chem. & Eng.* **2019**, *7*, 7743-7749.

[15] H. Zhong, L. A. Estudillo-Wong, Y. Gao, Y. Feng, N. Alonso-Vante, *ACS Appl. Mater. Interfaces* **2020**, *12*, 21605-21615.

[16] C. Shi, Y. Liu, R. Qi, J. Li, J. Zhu, R. Yu, S. Li, X. Hong, J. Wu, S. Xi, L. Zhou, L. Mai, *Nano Energy* **2021**, *87*, 106153.

[17] Z. Yang, X. Wang, M. Zhu, X. Leng, W. Chen, W. Wang, Q. Xu, L.-M. Yang, Y. Wu, *Nano Res.* **2021**, *14*, 4512-4519.

[18] M. Liu, J. Lee, T. C. Yang, F. Zheng, J. Zhao, C. M. Yang, L. Y. S. Lee, *Small Methods* **2021**, *5*, e2001165.

[19] F. Lu, K. Fan, L. Cui, B. Li, Y. Yang, L. Zong, L. Wang, *Appl. Catal. B-Environ.* **2022**, 313, 121464.

[20] H. Hu, J. Wang, B. Cui, X. Zheng, J. Lin, Y. Deng, X. Han, *Angew. Chem. Int. Ed.* **2022**, 61, e202114441.